EGU26-18500

Mantle temperatures from global seismic models: Uncertainties and limitations

Gabriel Robl[1], Bernhard S.A. Schuberth[1], Isabel Papanagnou[12], Christine Thomas[3]

1) LMU München, Dept. of Earth and Environmental Sciences, Germany. 2) University of Cambridge, Dept. of Earth Sciences, United Kingdom. 3) Universität Münster, Dept. of Physics, Germany. Contact: **gabriel.robl@lmu.de**

Sharing is encouraged

1. Motivation

- Geodynamic inverse models are emerging as valuable tools that allow to **link mantle flow histories to Earth's surface observations**, enabling to place tighter constraints on essential mantle properties
- They rely on accurate 3-D estimates of present-day mantle temperatures
  → need to be derived from seismic tomography
- Thermodynamic models of mantle mineralogy provide the **complex link between seismic velocities and temperatures**

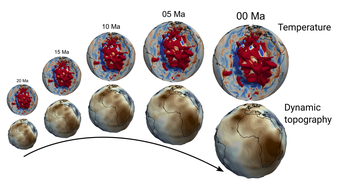

Evolution of temperature distributions of a geodynamic simulation together with resulting secondary observables, here dynamic topography. Comparing these observables against real surface observations through time allows to assess the validity of the geodynamic model. From *Colli et al., 2018.*

Inherent uncertainties when deriving mantle temperatures from tomography:

→ Mineralogical uncertainties
→ Limited tomographic resolution
→ Anelastic correction
→ Assumed bulk composition

2. Synthetic approach

How well can we predict the present-day thermal mantle structure from seismic tomography?

We employ a **synthetic closed-loop** approach, combining a **geodynamic model** with **thermodynamic models of mantle mineralogy** and **tomographic filtering**:

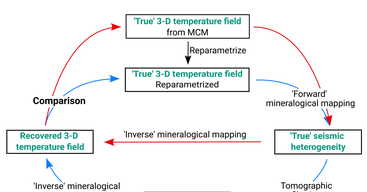

Schematic setup of the closed-loop, starting from a 3-D temperature field of an Earth-like mantle circulation model (MCM).

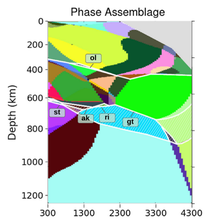

P-T-dependent stable phase assemblage for a pyrolite composition computed with *MMA-EoS*. From *Papanagnou et al., 2022.*

Non-linear mineralogical mapping: Linking thermal and seismic mantle structure

We convert between temperature and seismic velocity using mineralogical lookup tables computed with MMA-EoS *(Chust et al., 2017)* for a pyrolite composition, including a correction for anelasticity. For the 'inverse' mapping from seismic velocity to temperature, the **original** mineralogical model and **two reduced-complexity variants** are tested:

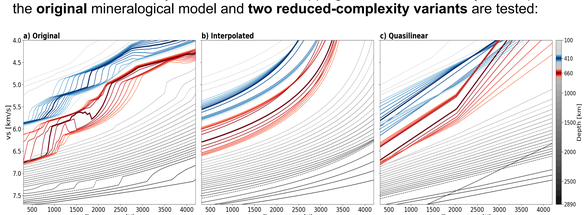

Relation between shear-wave velocity and temperature of the three mineralogical model representations used for the mapping from seismic velocity to temperature. Each line represents the relation at one discrete depth, with dashed lines indicating multiples of 500 km. Depth ranges around the prominent phase transitions at 410 and 660 km depth are highlighted for clarity.

3. Temperature uncertainty

'Perfect' seismic resolution

The resulting uncertainties in temperature are assessed by comparing the recovered temperature field with the 'true' reference model. The **influence of the mineralogical representation** alone is isolated by omitting tomographic filtering, thereby simulating an idealized scenario of 'perfect' seismic resolution and data coverage.

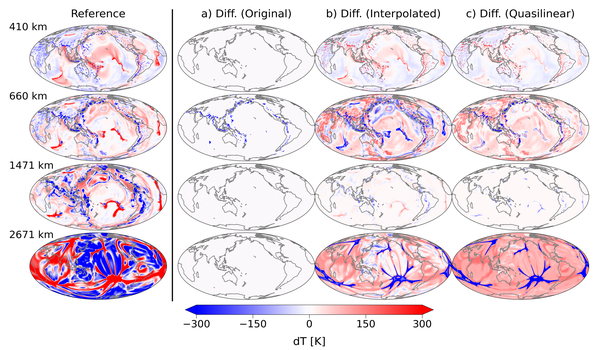

Temperature anomalies of the reference mantle circulation model and the corresponding point-wise differences with the recovered temperature fields are shown for all three mineralogical representations without tomographic filtering.

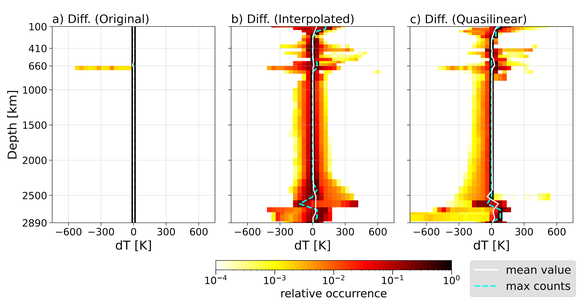

Histograms of point-wise temperature recovery errors for each inverse mineralogical mapping option in the idealized case of perfect seismic resolution.

Tomographic filtering: Making geodynamic and tomographic models comparable

To enable a fair quantitative comparison between seismic tomography and geodynamic models, we need to account for **effects of uneven data coverage and damping** through tomographic filtering:

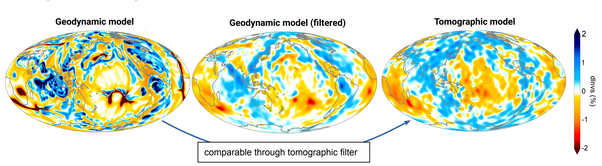

Depth slices of shear-wave variations of a geodynamic model (left) and a tomographic model (right). After tomographic filtering (middle), the imaged structures become comparable in terms of their length-scales and amplitudes.

We have four tomographic filters: **LLNL-G3D-JPS** (*Simmons et al. 2015, 2019*), **S40RTS** (*Ritsema et al. 2011*), **S20RTS** (*Ritsema et al. 1999*), **SP12RTS** (*Koelemeijer et al. 2016*).

Limited tomographic resolution

When including tomographic filtering in the closed-loop, we can assess the **combined uncertainty due to limited tomographic resolution and mineralogical complexities**:

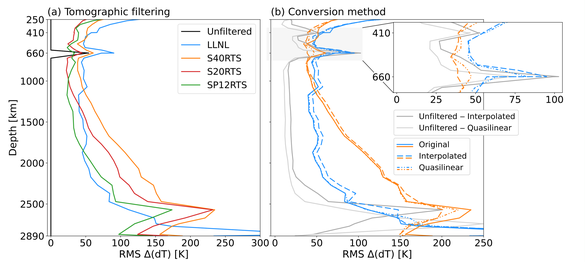

RMS-error of the recovered temperatures with application of different tomographic filters. (a) Comparison of the results with all four tomographic filters together with the original mineralogy. (b) Comparison of the inverse mineralogical mapping options in combination with two selected filters.

Uncertain anelastic correction

Both forward and inverse mineralogical mapping require an anelastic correction (AC), which can be controlled individually in our synthetic setup. We test two end-member scenarios: AC applied only to the **forward** mapping (**underestimation** of anelastic effects) and AC applied only to the **inverse** mapping (**overestimation** of anelastic effects).

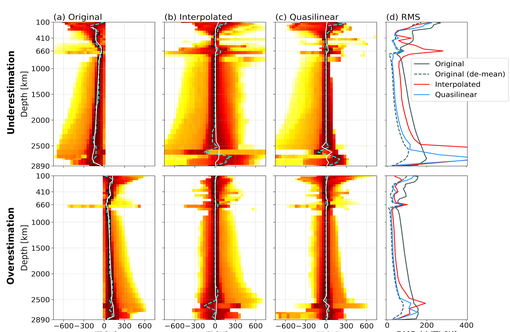

Histograms and RMS-curves of temperature-error with under- and overestimated anelastic correction without tomographic filtering.

Overestimating the anelastic correction to seismic velocities generally produces smaller average errors than underestimated anelastic effects.

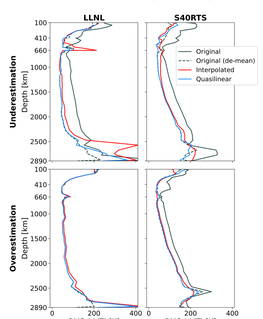

Including tomographic filtering

Accounting for realistic tomographic resolution brings the two end-member results into closer agreement. Nevertheless, overestimating the anelastic correction remains the more reliable choice, particularly for model *LLNL*.

4. Potential dynamic implications

At 660 km depth, different **phase transitions with opposite effects on buoyancy** can become dominant depending on temperature:

T < 1200 K: **Stishovite** ak+fp=st (exothermic) | 1200 K < T < 2150 K: **Ringwoodite** ri+br=fp (endothermic) | T > 2150 K: **Garnet** gt=br (exothermic)

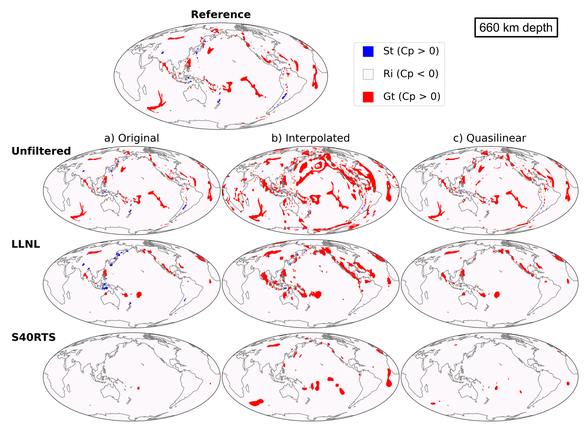

Distribution of the dominant phase transitions at 660 km depth depending on the temperature fields recovered with different tomographic filters and the three options for the mineralogical inverse mapping.

In geodynamic simulations that explicitly account for phase transition effects, errors in the recovered temperatures could therefore **significantly alter the buoyancy field around the 660**.

5. Conclusions

- Uncertainty of mantle temperatures inferred from tomographic models
  → Depth-dependent average errors of 50–200 K, depending on tomographic resolution
  → Additional systematic errors in the vicinity of phase transitions
- Overestimating the effects of anelasticity is more reliable than underestimation
- Potential dynamic implications due to 'activation' of wrong phase transitions with modern formulations of compressibility
- Intricate interplay between tomographic resolution and mineralogy – Best conversion strategy depends on requirements and the tomographic model
- Results are published in Robl *et al.* (2025)

Robl et al. (2025)

References

1. Robl, G., Schuberth, B.S.A., Papanagnou, I. & Thomas, C., 2025. From seismic models to mantle temperatures: Uncertainties related to mineralogical complexities and limited tomographic resolution, Geophys. J. Int., 241, 2022–2026.
2. Colli, L., Ghelichkhan, S., Bunge, H.-P. & Oeser, J., 2018. Retrodictions of mid Paleogene mantle flow and dynamic topography in the Atlantic region from compressible high resolution adjoint mantle convection models: sensitivity to deep mantle viscosity and tomographic input model, Gondwana Res., 53, 252–272.
3. Papanagnou, I., Schuberth, B.S.A. & Thomas, C., 2022. Geodynamic predictions of seismic structure and discontinuity topography of the mantle transition zone, Geophys. J. Int., 234(1), 355–378.
4. Chust, T.C., Steinle-Neumann, G., Dolejš, D., Schuberth, B. S.A. & Bunge, H.-P., 2017. MMA-EoS: a computational framework for mineralogical thermodynamics, J. Geophys. Res. Solid Earth, 122(12), 9881–9920.
5. Koelemeijer, P., Ritsema, J., Deuss, A. & van Heijst, H.J., 2016. SP12RTS: a degree-12 model of shear- and compressional-wave velocity for Earth's mantle, Geophys. J. Int., 204(2), 1024–1039.
6. Ritsema, J., van Heijst, H.J. & Woodhouse, J.H., 1999. Complex shear wave velocity structure imaged beneath Africa and Iceland, Science, 286(5446), 1925–1928.
7. Ritsema, J., Deuss, A., van Heijst, H.J. & Woodhouse, J.H., 2011. S40RTS: a degree-40 shear-velocity model for the mantle from new Rayleigh wave dispersion, teleseismic traveltime and normal-mode splitting function measurements, Geophys. J. Int., 184(3), 1223–1236.
8. Simmons, N.A., Myers, S.C., Johannesson, G., Matzel, E. & Grand, S.P., 2015. Evidence for long-lived subduction of an ancient tectonic plate beneath the southern Indian Ocean, Geophys. Res. Lett., 42(21), 9270–9278.
9. Simmons, N.A., Schuberth, B.S.A., Myers, S.C. & Knapp, D.R., 2019. Resolution and covariance of the LLNL-G3D-JPS global seismic tomography model: applications to travelttime uncertainty and tomographic filtering of geodynamic models, Geophys. J. Int., 217(3), 1543–1557.